<Original Paper>

Journal of the Korean Society for Nondestructive Testing, Vol. 35, No. 3: 206-214, 2015
ISSN 1225-7842 / eISSN 2287-402X http://dx.doi.org/10.7779/JKSNT.2015.35.3.206

NDE of Low-Velocity Impact Damage in GFRP Using Infrared Thermography Techniques

Ghiseok Kim*, Kye-Sung Lee**, Hwan Hur**, Sun-Jin Kim**, Geon-Hee Kim**†

Abstract In this study, low-velocity impact damage (LVID) in glass fiber reinforced plastic (GFRP) was investigated using pulse thermography (PT) and lock-in thermography (LIT) techniques. The main objective of this study was to evaluate the detection performance of each technique for LVID in GFRP. Unidirectional and cross-ply GFRPs were prepared with four energy levels using a drop weight impact machine and they were inspected from the impact side, which may be common in actual service conditions. When the impacted side was used for both inspection and thermal loading, results showed that the suggested techniques were able to identify the LVID which is barely visible to the naked eye. However, they also include limitations that depend on the GFRP thickness at the location of the delamination produced by the lowest impact energy of five joule.

Keywords: Low-Velocity Impact Damage, Glass Fiber Reinforced Plastic, Pulse Thermography, Lock-in Thermography

1. Introduction

Composite materials such as glass fiber reinforced plastic (GFRP) or carbon fiber reinforced plastic (CFRP) have the several advantages which are high strength, stiffness, light weight and good resistance to impact damage and chemical substance as well as the low-priced production cost. These features make such material attractive for diverse industries such as airplane, vehicle and ship. However, some properties of composite material can be degraded when this material is exposed to some types of damages including delamination, matrix cracking and debond. Especially a delamination can be significant one because the composite materials inherently have a structural vulnerability in the depth direction which result in the decrease of compression strength of them [1-3].

Delamination can be induced by a result of low-velocity impact (LVID) which occurred during the production, in-operation and repair works. LVID in composite materials can be rarely visible from an impact applied side but extended on the opposite side or in subsurface. Moreover, impacted side can be the only side which is able to maintenance on the spot field. This makes the inspection of LVID in com- posite materials as a hard work. Thus, various nondestructive inspection methods have been studied such as interferometric, thermal infrared, ultrasonic, X-ray radiographic and acoustic techniques [4-9].

As the one of optical imaging techniques, an infrared thermography method was consistently used due to its merits such as nondestructive, non-contacting, scalable full-field measurement. Basically, this technique measures the thermal response of material when it exposed to a possible excitation. Pulse thermography (PT) is one of active infrared thermography technique and it shows the failure of material by measuring the

[Received: June 1, 2015, Revised: June 22, 2015, Accepted: June 23, 2015] *Department of Biosystems Engineering, Seoul National University, 599 Gwanak-ro, Gwanak-gu, Seoul, 151-921, Korea, **Center for Analytical Instrumentation Development, Korea Basic Science Institute, 169-148 Gwahak-ro, Yuseong-gu, Daejeon, 305-806, Korea †Corresponding Author: kgh@kbsi.re.kr

thermal emissions from it after it was thermally excited. The size or shape of detected failure can be estimated using the measured thermal image through already known spatial resolution of lens and detector. Moreover, the quantitative estimation of defects such as depth and shape can be predicted by the post-processing of measurements. Meola et al. [10] has showed the geometrical effects of diameter, depth and thickness of failures in composite materials using the infrared thermographic method and revealed that a significant point in detectability was the thickness of them.

PT measures the temperature differences between defect and intact area to isolate the hidden defects in a sample. However, the temperature differences result not only from hidden defects, but also from the emissivity difference of material as well as non-uniform excitation conditions. Moreover, materials which consist of various thermal conductivities may result in poor image contrast because of its complicated thermal propagation. Thus, lock-in method has been employed to infrared thermography to increase its detection performance [11-16]. Lock-in thermography technique commonly uses a heating device or an ultrasonic transducer as a periodical excitation source and the calculated amplitude and phase of measured thermal signal shows a defect of materials such as the size and depth of the damage. Bates et al. [11] demonstrated and revealed the detection performance for several infrared nondestructive techniques through the inspection of a carbon fiber composite which commonly used in the aircraft. They showed that lock-in thermography technique was the best in the detection of impact damage. Moreover, pulsed thermography was fairly feasible for the detection of inclusions of it. Wu and Busse [12] has represented the working principle of lock-in thermography and showed that the technique can reduce some possible measurement disturbances including the reflections from optical device, local difference of material's emissivity as well as inhomogeneous conditions by excitation sources. Choi et al. [16] also have represented the spatial information such as size and position of hidden defects using LIT technique.

In this research, we evaluated PT and LIT techniques in order to demonstrate and reveal their working performance against the LVID in GFRP. In order to test these thermography techniques, four levels of impact damage were introduced into GFRP through a impact machine. Moreover, the estimated LVID results by PT and LIT have been compared with visual inspection results.

2. Infrared Thermography Techniques

2.1 Pulse Thermography(PT)

Principle of PT is shown in Fig. 1. The specimen surface is submitted to a thermal pulse using an instantaneous flash or halogen lamp. The duration of the thermal exposure can be determined from milliseconds to a few seconds depending on the thermal property of test material and its defect. After the thermal wave comes into contact with the specimen's surface, it propagates through the specimen. As time elapses, defect areas show the higher or lower temperature with respect to intact area. Then the temperature change on the surface or in the

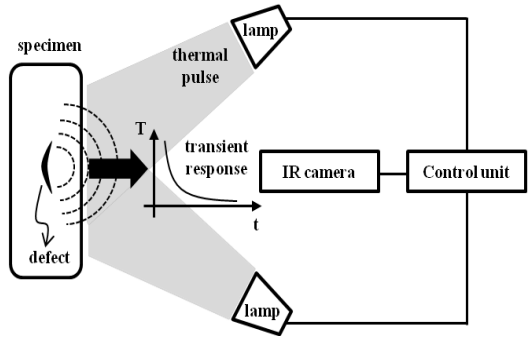

Fig. 1 Working principle of pulse thermography

subsurface is monitored by an infrared camera. A sequence of such thermal images can be further processed to estimate the size and depth of the defects. Moreover, some noise in the thermal images, which is commonly from hardware and environments, can be removed through the image processing such as logarithmic time evolution and least-squares fit method. Additional image processings such as convolution, image subtraction and contrast stretching can be employed to enhance the visibility of defects.

Plotting the logarithm of the sequential data sets of the temperature at each pixel shows a straight line characteristic which has a slope of -0.5. However, when the thermal wave encounters a defect, a deviation from the characteristic straight line occurs. By focusing on the nonlinearity of a characteristic straight line at single pixel, it is possible to identify an internal discontinuity that means the defect. Furthermore, the time information of the nonlinearity can be used as a function of the defect depth. Thus, it is able to calculate the depth of defects and thickness of material by analyzing the characteristic transit time information. Reversely, if we know the depth or thickness of defects, the thermal properties such as diffusivity of the sample can be estimated [17].

In the PT, we used the thermographic signal reconstruction (TSR) method which is expressed by Eq. (1) to enhance the detection sensitivity. This method is effective for the cooling image after a specimen was heated by a thermal pulse because a least-squares fit of a low-order polynomial to the logarithmic time history can excludes the extraneous non-thermal components, accentuates the defect signal within the measured signal, highlights the defect signal that deviate from typical cooling behavior.

$$\ln[T(t)] = \sum_{n=0}^{N} a_n [\ln(t)]^n \quad (1)$$

where N is the order of the polynomial. For the intact area of specimen, the 1st derivative of Eq. (1) will be a constant value of -0.5. However, this value will be changed or be bounded by zero if the thermal wave encounters the defect which results in the discontinuity of constant value.

2.2 Lock-in Thermography (LIT)

Working principle of LIT is shown in Fig. 2. Periodical thermal wave propagates into the test sample and be reflected at the surface or inner surface which means the defect. The temperature modulation at the surface is modified by the thermal waves come from the inner surface or defects of the target and resulting interference of thermal wave is induced. Then the infrared detector measures the temperature by picking up a series of thermal images and reconstructs a modulated wave through measured thermal signals with a phase period of T/4 (where T is a period). Then, phase image and amplitude image *A(x,y)* can be obtained by Eq. (2),(3) [14,15].

$$\phi(x,y) = \arctan\left(\frac{S_1(x,y) - S_3(x,y)}{S_2(x,y) - S_4(x,y)}\right) \quad (2)$$

$$A(x,y) = \sqrt{(S_1(x,y) - S_3(x,y))^2 + (S_2(x,y) - S_4(x,y))^2} \quad (3)$$

where S_n are recorded images for one cycle.

Every pixel value of the resultant phase image which was obtained by Eq. (2) means the

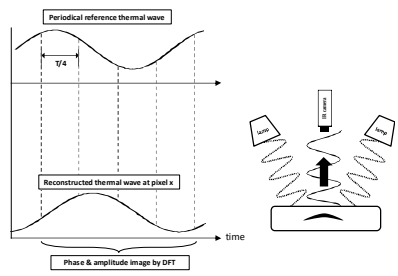

Fig. 2 Working principle of lock-in thermography

phase variation of the emitted thermal signal from intact and defect. Phase information is mainly preferred due to its robustness to non-uniform excitation condition and emissivity difference of the target surface.

3. Materials and Methods

Two GFRPs (Cyply FP-144, Cyply FP-43, Cytec Inc., USA) were used for research. FP-43 was crossply and FP-144 was unidirection product. The stacking sequences were $[0/90/0_9/90/0]$ for FP-144 unidirection and $[\bar{0}/90]_{6S}$ for FP-43 crossply. Fig. 3 shows the geometry of each material and dimensions are 100 × 100 × 3.3 mm for both specimens. Impact was introduced using a drop weight impact machine (Dynatup 9250HV, Instron Inc., USA) according to the ASTM D7136 test method. Specimens were tightly fixed using pneumatic device and the tup impactor (hemispherical tip with 6 mm diameter). Total mass of 6.625 kg was used to artificially make the impact damage into the test samples. Impact energies were ranged from 5, 10, 15 and 18 J by changing the drop height of dead weight. Fig. 4 shows the LVID on both impact applied side and opposite side of the GFRP test materials which were impacted with 18 J.

The DeltaTherm Infrared differential thermography system (DT1570, Stress Photonics Inc., USA) was used for the infrared thermography test. The camera utilizes a 320 × 256 InSb detector array with 3-5μm sensitivity and frame rate was 1,000 fps. Two halogen lamps (100 W of each) were used for thermal wave source. The camera to sample distance was 1.0 m and the halogen lamp to sample distance was 0.3 m. During the whole infrared thermography test, GFRP specimens were painted with flat black color and heated from impact side because the impact side is commonly accessible during in-service.

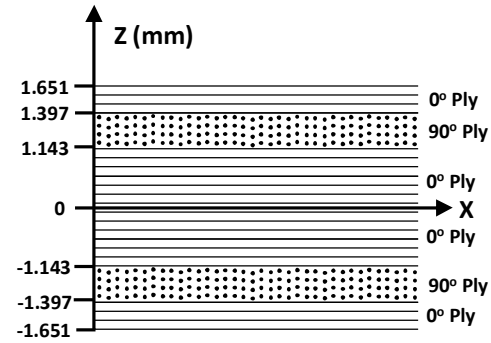

(a) Unidirection

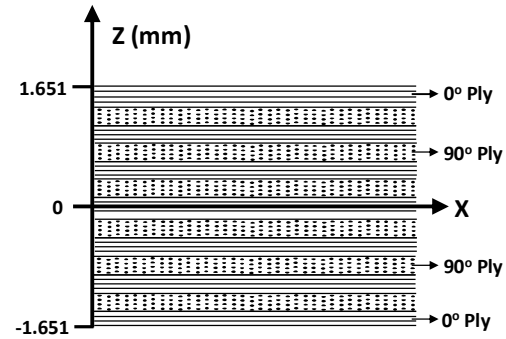

(b) Crossply

Fig. 3 Geometry of GFRP specimen

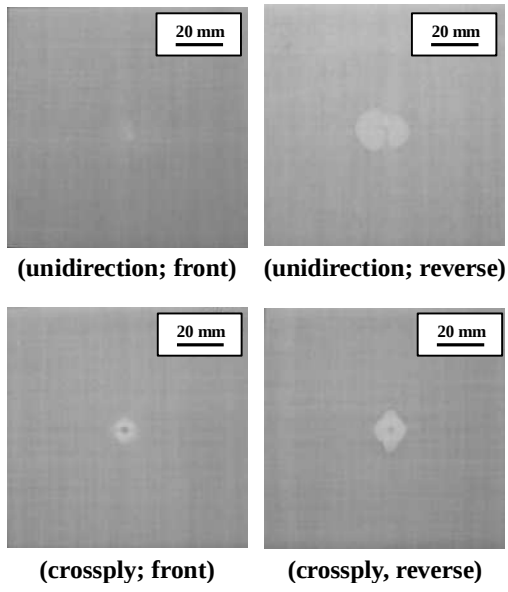

(unidirection; front) **(unidirection; reverse)**

(crossply; front) **(crossply, reverse)**

Fig. 4 LVID on GFRP specimens (impact energy: 18 J)

After all the infrared thermography test was done, black paint on specimens was cleaned and LVID on both sides of GFRP specimens were inspected with CCD camera to compare the LVID size and shape detected by visual inspection method with them which measured by infrared thermography methods. During the visual inspection, a series of image processing technique was employed to enhance the detection performance of LVID on specimens using Matlab (ver. 8.0, MathWorks, Natick, MA, USA). This works reduce the noises, detect the LVID edge boundary, and finally show the LVID shape and size on GFRP specimens. The flow chart of image processing is shown in Fig. 5. Fig. 6 shows the visual inspection results of LVID on both sides of GFRP specimens which were damaged by 18 J impact.

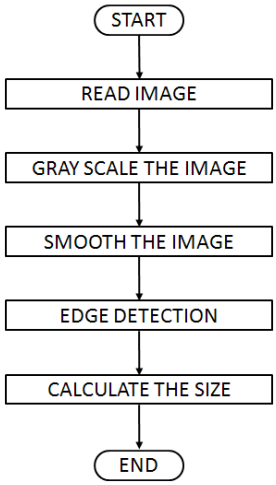

Fig. 5 Flow chart of image processing

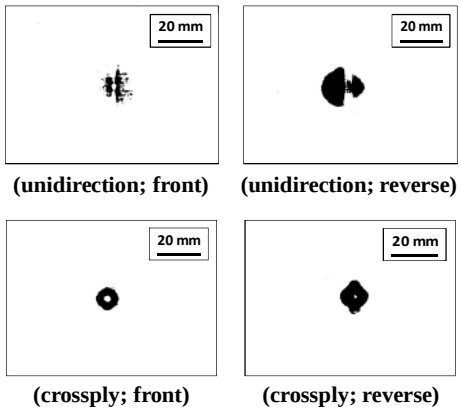

(unidirection; front) **(unidirection; reverse)**

(crossply; front) **(crossply; reverse)**

Fig. 6 Visual inspection results (impact energy: 18 J)

4. Results and Discussion

Fig. 7 and Fig. 8 show the LVID on impact applied side (front side) and opposite side by visual inspection method. And, the estimated damage sizes on both sides were summarized in Fig. 9. In case of visual inspection, black paint on GFRP specimens was clearly removed before. From the results of visual inspection, estimated damage size on opposite side was larger than that on front side and it was increased with increasing impact energy. However, the LVID on the opposite side of crossply with 5 J impact was not detected at all by visual inspection method.

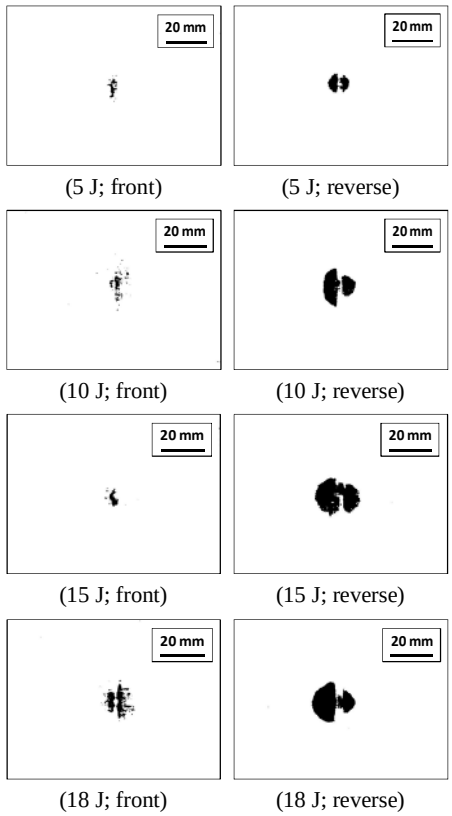

(5 J; front) (5 J; reverse)

(10 J; front) (10 J; reverse)

(15 J; front) (15 J; reverse)

(18 J; front) (18 J; reverse)

Fig. 7 Visual inspection results of LVID on unidirection GFRP

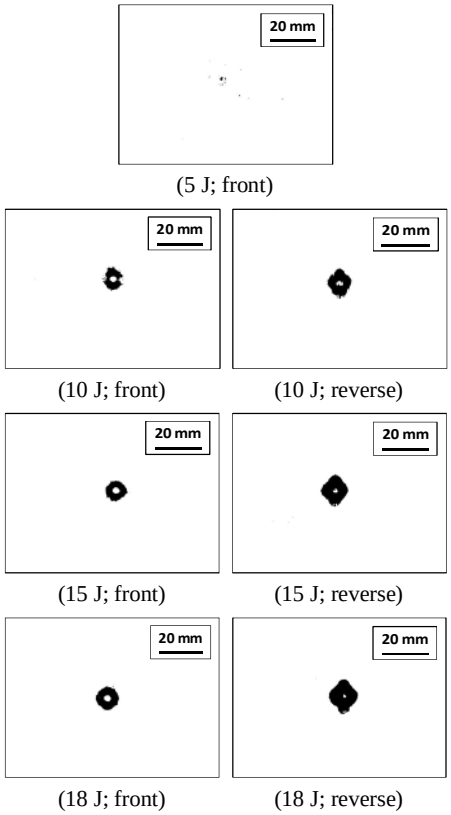

Fig. 8 Visual inspection results of LVID on crossply GFRP

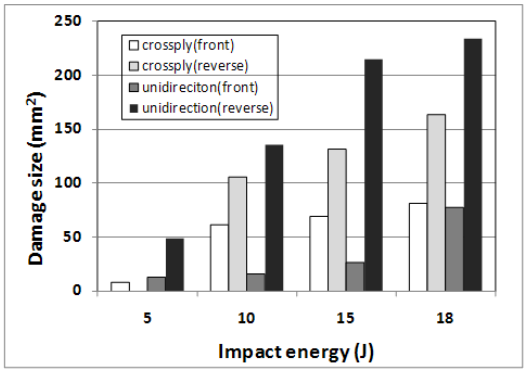

Fig. 9 Estimated LVID size by visual inspection

From the visual inspection results, LVID on the front side of unidirection was barely visible but it was clearly visible from opposite side and LVID size and shape which measured from both sides was quite different. In case of the unidirection GFRP specimens, it was estimated that the LVID on front side was mainly caused by matrix cracking or fiber breakage on 0^o fiber which are barely visible by human eye. However, the LVID on opposite side was easily visible by human eye because delamination on 90^o fiber was happened as a significant failure on opposite side or in subsurface. In case of the crossply GFRP specimens, LVID which caused by matrix cracking and delamination was clearly detected at both front and opposite side. For all specimens, LVID size at opposite was larger than that of front. Above results demonstrate that the impact energy which absorbed in GFRP specimens was increased through thickness and opposite side could be significantly damaged than front side by the propagation of impact energy.

Fig. 10 shows the results of PT for the LVID on crossply GFRP specimens which were heated by halogen lamps and inspected from front side. As shown in Fig. 10, LVID on crossply GFRP by 10 J, 15 J and 18 J impact was detected but any LVID was not detected in unidirection GFRP by the PT method. And, it was observed that the obtained LVID shape on crossply GFRP by PT was similar with the LVID shape on front side of crossply GFRP which measured by visual inspection method. This represents that the PT method could detect only the LVID on the front surface of crossply GFRP while it could not detect the defects on the opposite side or inner damages of both crossply and unidirection GFRP when they were damaged by low-velocity impact. From the results of PT test, it was revealed that the detection sensitivity of PT has some limitations for the detection of matrix cracking or fiber breakage which can be happened in the low-energy impacted GFRPs. I assumed that these limitations of PT method can be caused by low thermal conductivity of GFRP even though the barely visible impact damage can cause the serious failure in GFRP products.

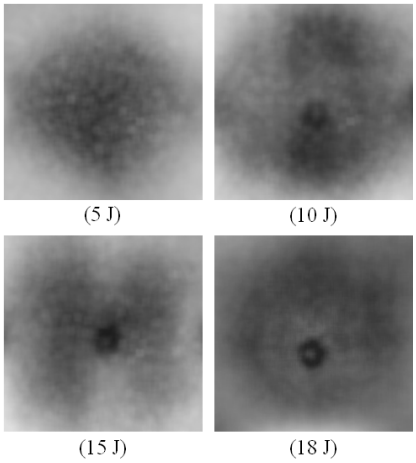

Fig. 10 Pulse thermography results against LVID on crossply GFRP

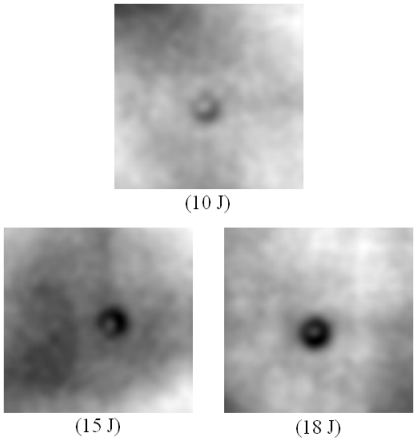

Fig. 11 Lock-in thermography results against LVID on crossply GFRP

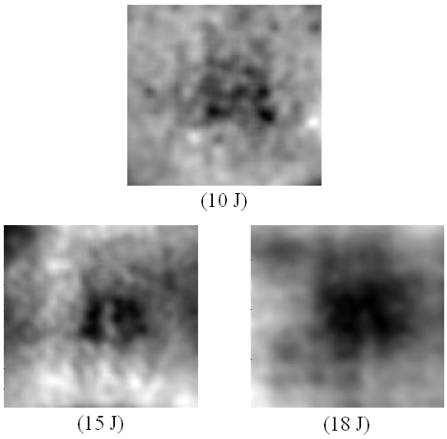

Fig. 12 Lock-in thermography results against LVID on unidirection GFRP

Fig. 11 shows the resultant phase images of LIT, and excitation frequency considered for lock-in thermography was 0.05 Hz. In case of the crossply GFRP specimens, LVIDs by 10 J, 15 J and 18 J impact were successfully detected but in case of the unidirection test, only the LVIDs by 15 J, 18 J impacts were detectable. However, it was shown that the detection sensitivity was improved by embedding the LIT technique into the NDE of LVID on the unidirection GFRP. The phase images shown in Fig. 11 and Fig. 12 represent the phase difference of each pixel which calculated from the modulated surface temperature by Eq. (2).

From the results, the enhanced detection sensitivity by LIT can be caused by the modulated thermal wave which can penetrate deeper into the specimen than single pulse thermal wave can. Moreover, the phase calculation method is relatively undisturbed by emissivity variations, and non-homogeneous heating and allows for a deep analysis. Herein, we discriminated the defects by calculating the phase difference in phase image. If the specific area (damaged area) has the pretty higher or lower phase value than surroundings or background, it was the damage area.

5. Conclusions

Visible inspection, pulse thermography and lock-in thermography NDE techniques were investigated to identify their detection performance and limitations for the unidirection and crossply GFRP specimens which were impacted by four different low energies. Experimental results showed that the LIT method was able to detect the LVID which exists as the matrix cracking and delamination for both unidirection and crossply GFRP specimens but PT method could not detected the LVID for unidirection GFRP from front inspection condition which can be commonly available in depot level.

In conclusion, both PT and LIT were proven to be useful method for a simple and quick investigation of impact damaged composite materials. However, detection sensitivity of LIT was better than that of PT for the LVID on unidirection GFRP. So LIT can be considered as a more useful method for NDE of the composite materials employed in industrial applications. Also, advantage of LIT is the detection sensitivity to the depth of a defect without troublesome post processing procedures. However, one limitation to LIT can be the selection of optimal frequency for the thermal wave modulation to detect relatively deep defects in thick target materials which have very low thermal conductivity.

Acknowledgment

This research was partially supported by the Korea Basic Science Institute Grant (D35500), and the R&D Convergence Program of MSIP (Ministry of Science, ICT and Future Planning) and ISTK (Korea Research Council for Industrial Science and Technology) of Republic of Korea (Grant B551179-12-04-00).

References

[1] K. L. Reifsnider, "Damage in Composite Materials," ASTM STP, Vol. 775, Philadelphia: American Society for Testing and Materials, (1982)

[2] S. Abrate, "Impact on Composite Structures," Cambridge: Cambridge University Press, (1998)

[3] W. J. Cantwell and J. Morton, "The impact resistance of composite materials - a review," *Composites*, Vol. 22, pp. 347-362 (1991)

[4] R. Ambu, F. Aymerich, F. Ginesu and P. Priolo, "Assessment of NDT interferometric techniques for impact damage detection in composite laminates," *Composite Science and Technology*, Vol. 66, pp. 199-205 (2006)

[5] M. O. W. Richardson, Z. Y. Zhang, M. Wisheart, J. R. Tyrer and J. Petzing, "ESPI non-destructive testing of GRP composite materials containing impact damage," *Composites Part A*, Vol. 29A, pp. 721-729 (1998)

[6] R. Ruzek, R. Lohonka and J. Jironc, "Ultrasound C-Scan and shearography NDI techniques evaluation of impact defects identification," *NDT&E International*, Vol. 39, pp. 132-142 (2006)

[7] K. Diamanti, J. M. Hodgkinson and C. Soutis, "Detection of low-velocity impact damage in composite plates using Lamb waves," *Structural Health Monitoring*, Vol. 3, pp. 33-41 (2004)

[8] F. Aymerich and W. J. Staszewski, "Impact damage detection in composite laminates using nonlinear acoustics," *Composites Part A*, Vol. 41, pp. 1084-1092 (2009)

[9] C. Potel, T. Chotard, J. F. Belleval and M. Benzeggagh, "Characterization of composite materials by ultrasound methods: modelization and application to impact damage," *Composites Part B*, Vol. 29, pp. 159-169 (1998)

[10] C. Meola, G. M. Carlomagno and L. Giorleo, "Geometrical limitations to detection of defects in composites by means of infrared thermography," *Journal of Nondestructive Evaluation*, Vol. 23, pp. 125-132 (2004)

[11] D. Bates, G. Smith, D. Lu and J. Hewitt, "Rapid thermal non-destructive testing of aircraft components," *Composites Part B*, Vol. 31, pp. 175-185 (2000)

[12] D. Wu and G. Busse, "Lock-in thermography for nondestructive evaluation of materials," *Revue Générale de Thermique*, Vol. 37, pp. 693-703 (1998)

[13] D. Wu, A. Salerno, B. Schonbach, H. Hallin

and G. Busse, "Phase-sensitive modulation thermography and its applications for NDE," *Proc. SPIE 3056*, Orlando, Florida, USA, pp. 176-182 (1997)

[14] J. H. Park, M. Y. Choi and W. T. Kim, "Shearing phase lock-in infrared thermography for defects evaluation of metallic material specimen," *Journal of the Korean Society for Nondestructive Testing*, Vol. 30, pp. 91-97 (2010)

[15] M. Y. Choi, K. S, Kang, J. H. Park, W. T. Kim and K. S. Kim, "Quantitative determination of a subsurface defect of reference specimen by lock-in infrared thermography," *NDT&E International*, Vol. 41, pp. 119-124 (2008)

[16] W. Bai and B. S. Wong, "Evaluation of defects in composite plates under convective environments using lock-in thermography," *Meas. Sci. Technol.*, Vol. 12, pp. 142-150 (2001)

[17] Y. Y. Hung, Y. S. Chen, S. P. Ng, L. Liu, Y. H. Huang, B. L. Luk, R. W. L. Ip, C. M. L. Wu and P. S. Chung, "Review and comparison of shearography and active thermography for nondestructive evaluation," *Materials Science and Engineering R*, Vol. 64, pp. 73-112 (2009)